

# Dynamically Generated Patterns in Dense Suspensions of Active Filaments

K. R. Prathyusha,<sup>1</sup> Silke Henkes,<sup>2</sup> and Rastko Sknepnek<sup>1,3</sup>

<sup>1</sup>*School of Science and Engineering, University of Dundee, Dundee, DD1 4HN, United Kingdom*

<sup>2</sup>*Institute of Complex Systems and Mathematical Biology, Department of Physics,  
University of Aberdeen, Aberdeen AB24 3UE, United Kingdom*

<sup>3</sup>*School of Life Sciences, University of Dundee, Dundee, DD1 5EH, United Kingdom\**

(Dated: August 12, 2016)

Motivated by recent experiments on suspensions of active microtubule bundles driven by molecular motors we use Langevin dynamics simulations to study a dense planar layer of active semi-flexible filaments. Using the strength of active force and the thermal persistence length as parameters, we map the phase diagram and identify several non-equilibrium states in this system. In addition to a flowing melt phase, we observe that for sufficiently high activity, collective flow accompanied by the emergence of local polar and nematic order appears in the system. Most strikingly, we identify an activity-driven cross-over from a state of coherently flowing bundles of filaments to a phase with no global flow, formed by filaments coiled into rotating spirals. This suggests a mechanism where the system responds to activity by changing the shape of active agents, an effect with no analogue in systems of active particles without internal degrees of freedom.

PACS numbers: 47.57.-s, 61.25.H-

**Introduction.** Out of equilibrium behaviour of actively driven filaments has been a focus of vigorous research [1, 2]. For example, the dynamics of cytoskeletal actin filaments are characterised by a constant supply of mechanical energy by myosin motor proteins, which hydrolyse ATP to slide along actin chains. This directed motion is integral to cell migration. Many cellular processes can be mimicked by *in-vitro* experiments on motility assays. Particularly interesting motion patterns arise in mixtures of microtubule bundles propelled by ATP driven kinesin motors [3–5], where flow is accompanied by a spontaneous generation of topological defects [3], so-called active turbulence [6, 7] and the orientational order of motile defects [5].

In the dilute regime, steric interactions play a limited role and insights can be gained by studying individual filaments [8–10] or hydrodynamic equations derived from microscopic models that consider only binary collisions [11, 12]. Studies of individual active filaments pivoting around one clamped end show that activity can drive conformational instabilities [13], with a spiralling pattern [10, 14, 15] being a prominent feature. Balancing the bending moment with the torque produced by the active force shows [14, 15] that activity increases the tendency of the filament to buckle, thus reducing its persistence length. Similar effects have also been observed in models that treat activity as time-correlated random forces [16, 17]. Collective effects in dense suspensions of active semi-flexible filaments are, however, still poorly understood.

In this paper we explore the non-equilibrium phases of self-propelled semi-flexible filaments confined to move on a flat substrate. We focus on the dense regime, where steric effects cannot be ignored but hydrodynamic interactions are negligible [18]. We map a non-equilibrium phase diagram as a function of activity and stiffness of

filaments and identify five distinct phases: melt, flowing melt, swirling, segregated, and rotating spiral phases. In particular, we observe that filaments adjust their conformation to accommodate the activity leading to the disappearance of the segregated phase in the high activity regime. This is contrary to the behaviour observed in models of structureless active particles where motility induced phase segregation [19] (MIPS) becomes more prominent with increasing activity [20].

**Model.** We adapt the model introduced recently in [9] to study conformations of a single semi-flexible filament under the influence of an active force of constant magnitude acting along its contour. Our system consists of  $M$  such filaments confined to a periodic square region of length  $\ell$  with each filament modelled as a chain of  $N$  beads of diameter  $\sigma$ . The packing fraction  $\phi = (MN\sigma^2\pi)/4\ell^2$  is set to  $\phi = 0.64905$ , well below both the triangular lattice and random close packing.

Interactions are modelled with bonded and short-range non-bonded pair potentials,  $U = U_B + U_{NB}$ . Bonded interactions,  $U_B$ , account for both chain stretching, modelled with the FENE bond potential [21],  $U_s(r_{ij}) = -1/2k_b R_0^2 \ln(1 - (r_{ij}/R_0)^2)$  and bending, modelled with an angle potential  $U_b = \kappa(\theta - \pi)^2$ . Here,  $\kappa$  is the bending stiffness,  $\theta$  is the angle between three consecutive beads,  $R_0 = 1.3\sigma$  is the maximum bond length,  $k_b = 3300k_B T/\sigma^2$  is the bond stiffness (making the chain effectively non-stretchable), and  $r_{ij} = |\mathbf{r}_i - \mathbf{r}_j|$  is the distance between beads at positions  $\mathbf{r}_i$  and  $\mathbf{r}_j$ . For a stiff filament, the bending stiffness  $\kappa$  in the discrete model is related to the continuum bending stiffness,  $\tilde{\kappa}$ , as  $\kappa \approx \tilde{\kappa}/2b$ , where  $b$  is the average bond length. Non-bonded interactions,  $U_{NB}$ , account for steric repulsions and are modelled with the Weeks-Chandler-Anderson potential [22],  $U_{WCA}(r_{ij}) = 4\epsilon((\sigma/r_{ij})^{12} - (\sigma/r_{ij})^6 + 1/4)$ , with

$\varepsilon$  measuring the strength of steric repulsion. These parameters lead to  $b \approx 0.86\sigma$ , which ensures that filaments do not intersect. Finally,  $L = (N - 1)b$  is the mean filament length and  $T$  is set to  $0.1\varepsilon/k_B$ .

The active force on bead  $i$  is modelled as  $\mathbf{f}_i^a = f_p(\mathbf{t}_{i-1,i} + \mathbf{t}_{i,i+1})$ , which mimics active driving produced by a homogeneous distribution of molecular motors. Here,  $f_p$  is the strength of the force and  $\mathbf{t}_{i,i+1} = \mathbf{r}_{i,i+1}/r_{i,i+1}$  is the tangent vector along the bond connecting beads  $i$  and  $i + 1$ ; end beads have only contributions from one bond. The filament dynamics is described by Langevin equations of motion:

$$m_i \ddot{\mathbf{r}}_i = \mathbf{f}_i^a - \gamma \dot{\mathbf{r}}_i - \nabla_{\mathbf{r}_i} U(r_{ij}) + \mathbf{R}_i(t), \quad (1)$$

where  $m_i = 1$  is the mass of bead  $i$ . Time is measured in units of  $\tau = \sqrt{m\sigma^2/\varepsilon}$ .  $\mathbf{R}_i(t)$  is delta-correlated thermal noise with zero mean and variance  $\langle \mathbf{R}_i(t) \cdot \mathbf{R}_j(t') \rangle = 4\gamma k_B T \delta_{ij} \delta(t - t')$ , with  $\gamma = k_B T \tau / \sigma^2$ . Eqs. (1) were integrated with time step  $\Delta t = 10^{-3}\tau$  using LAMMPS [23], with an in-house modification to include the active propulsion force. A typical configuration contained  $\approx 50000$  beads and was generated by placing chains at random into the simulation box ( $\ell = 250\sigma$ ), making sure that there were no intersections. This configuration was then relaxed for  $10^4\tau$ , followed by a production run of  $10^5\tau$ .

Our key parameters are the degree of polymerisation,  $N \in \{5, 10, 25, 50\}$ , the filament stiffness,  $\kappa = 1 - 20 k_B T$  and the magnitude of the active force,  $f_p = 2 \times 10^{-4} - 1 k_B T / \sigma$ . We identify two dimensionless numbers: the relative filament stiffness  $\xi_p/L$ , where  $\xi_p = \tilde{\kappa}/k_B T = 2b\kappa/k_B T$  is the thermal persistence length and the active Péclet number,  $Pe = f_p L^2 / \sigma k_B T$ . As previously shown [13, 15], the flexure number,  $\mathfrak{F} = f_p L^3 / \kappa = \sigma^2 Pe / (\xi_p/L)$ , controls the buckling instabilities of a single active filament. Meanwhile, the Péclet number controls the onset of MIPS [20].

*Results.* While there are similarities with the behaviour of a single active filament [10], the combination of self-avoidance and flexibility in dense suspensions leads to interesting collective behaviour even in the absence of any explicit aligning interactions. In FIG. 1 we show the non-equilibrium phase diagram in the  $\xi_p/L$  vs.  $Pe$  plane with snapshots of the simulations in the four main non-equilibrium phases shown in FIG. 2 (see also movies in [24]). The nature of the flow in the system can be characterised by the mean squared displacement (MSD) of the centre of mass of filaments, averaged over all filaments (FIG. 3a). Without activity ( $Pe = 0$ ), after the usual short time ballistic relaxation, the MSD curve shows subtly sub-diffusive dynamics with exponent  $\approx 0.8$  indicating glassy-like behaviour [24]. Activity, however, introduces flow. For low activity, steric repulsions dominate and the system resembles a conventional polymer melt where activity acts only as a weak perturbation. For flexible filaments ( $\xi_p/L \lesssim 0.1$ ) at  $Pe \gtrsim 1$  the diffusion

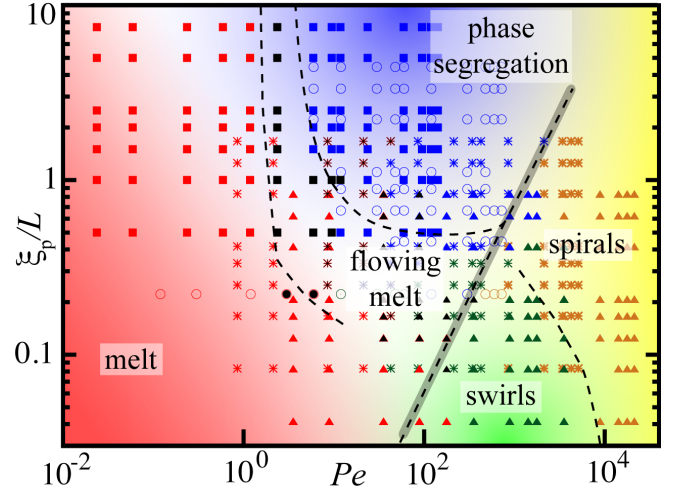


FIG. 1. (Colour online) Non-equilibrium phase diagram for  $\xi_p/L$  vs.  $Pe$  at packing fraction  $\phi = 0.64905$ . Symbols mark individual simulations for different filament lengths:  $N = 5$  ( $\blacksquare$ ),  $N = 10$  ( $\circ$ ),  $N = 25$  ( $*$ ) and  $N = 50$  ( $\blacktriangle$ ), with phases coded by colour. Different phases were identified by visually inspecting each individual run. Crossovers between phases are indicated by shading. Dashed lines indicate rough boundaries between phases and serve as a guide to the eye. The grey-shaded bar indicates the threshold to spiralling, set by the flexure number  $\mathfrak{F} \approx 10^3$  [10].

coefficient increases linearly with Péclet number (inset, FIG. 3b), in qualitative agreement with the predictions of a simplified model for a fully-flexible active chain subject to Rouse dynamics [24]. Stiffer filaments, on the other hand, transition from subdiffusive to superdiffusive flow at  $Pe \approx 1$ . For longer filaments, in this “flowing melt” regime, one observes  $\pm 1/2$  topological defects (FIG. 2a) similar to those seen in the experiments of Sanchez, *et al.* [3]. The defect core consists of filaments bent into hair-pin configurations. Defect motion is very slow and is facilitated by filaments sliding along their contour.

For  $Pe \approx 10^2 - 10^4$  and  $\xi_p/L \lesssim 0.2$  the system is in the “swirling” state (FIG. 2b). Already flexible filaments are actively pushed against each other enhancing shape fluctuations which prevents formation of large-scale flow patterns. If the stiffness is increased ( $\xi_p/L \gtrsim 0.2$ ), large bends become costly and at sufficiently high Péclet numbers,  $Pe \gtrsim 10$ , similar to the Péclet threshold in MIPS of self-propelled particles [20], the system crosses over into a phase-segregated state (FIG. 2c) characterised by filaments aligning and flowing as a coherent bundle. The mechanism that leads to this behaviour can be explained as follows. When multiple filaments collide with each other in a “head-to-front” manner, steric interactions align them into bundles that propagate coherently [9]. This, however, happens only if filaments are sufficiently stiff since for soft filaments, fluctuations in the direction of motion prevent them from bundling [24]. Bundles break up due to collisions with filaments in surrounding

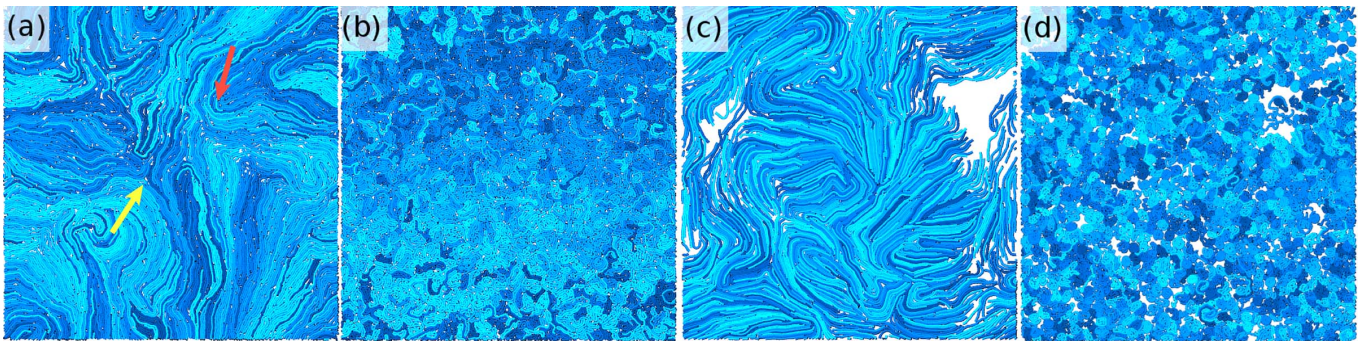


FIG. 2. (Colour online) Snapshots of simulations for  $N = 50$  in four non-equilibrium phases: (a) flowing melt ( $\xi_p/L = 0.2$ ,  $Pe = 35.5$ ), (b) swirl ( $\xi_p/L = 0.04$ ,  $Pe = 177.58$ ), (c) segregated phase ( $\xi_p/L = 0.82$ ,  $Pe = 355.16$ ) and (d) spirals ( $\xi_p/L = 0.04$ ,  $Pe = 17757.8$ ). Individual filaments are marked by a different shade. Arrows in (a) point to examples of  $+1/2$  (red) and  $-1/2$  (yellow) topological defects. White areas in (c) are regions devoid of filaments, indicating substantial density fluctuations.

bundles and thermal noise. The motion of the bundles is accompanied by substantial density fluctuations (white regions in FIG. 2c), akin to those seen in the MIPS phase of self-propelled disks. Once formed, the entire bundle retains its direction over an extended period of time, in some cases comparable to the length of the entire simulation. This can be seen in the MSD curves (FIG. 3a), which show wide regions of persistent,  $\sim t^2$ , behaviour. At long times, however, the direction of motion of bundles decoheres and diffusive behaviour is recovered. It is interesting that the transition time,  $\tau_c$ , of the onset of diffusive behaviour *reduces* with activity as  $\tau_c \sim (Pe)^{-\zeta}$ , with  $\zeta \approx 0.9 - 1.5$  where exponent  $\zeta$  increases with filament stiffness [24]. A similar activity-dependent decrease of  $\tau_c$  has been observed in single-filament studies [10]. Finally, as expected, the size of bundles depends on the system density (see movies in [24]).

The “phase segregated” state is not stable for large Péclet numbers. The onset of the instability is controlled by the flexure number,  $\mathfrak{F}$  (grey-shaded region in FIG. 1). We find a similar threshold,  $\mathfrak{F} \approx 10^3$ , as in the single-filament case [10]. For  $Pe \gtrsim 10^3$ , the coherently moving bundles dissolve and the system regains a nearly uniform density. The structure of this state is markedly different from the low activity case. Most filaments curl into long-lived spirals (FIG. 2d). While the head bead of the filament is always in the centre there is no preferred direction of the rotation, i.e., there is no global chirality. Centres of spirals move diffusively (FIG. 3a). If the system density is reduced, the state resembles a weakly interacting gas of rotating spirals [24]. It is interesting to ask why the system prefers this unusual spiralling state, as opposed to, e.g., a configuration where perfectly aligned fully stretched filaments flow parallel to each other, which would be preferential energetically. We argue that it is ultimately connected to the conformational entropy of the chains: Straight filament configurations are entropically costly and spontaneous shape fluctuations would affect the entire flow. On the other hand, the entropically favourable coiled conformations are not compatible with

the self-propulsion which prefers coherent motion with a constant speed  $\approx f_p/\gamma$ . Therefore, the system balances these two competing effect by selecting filament conformations that “trap” most activity into circular motion. This mechanism has no analogue in systems of simple structureless active agents and owes its existence solely to the extended nature of the filaments, as can also be seen by reducing  $N$ , which leads to the disappearance of the spiralling state [24].

One of the identifying features of self-propelled filaments is the reduction of the effective bending stiffness manifested as the decrease of the thermal persistence length,  $\xi_p$ . The active persistence length,  $\xi_p^a$ , is determined by fitting the tangent-tangent correlation function  $\langle \mathbf{t}(s) \cdot \mathbf{t}(0) \rangle$  to  $\exp(-s/\xi_p)$ , where  $s$  measures the position along the contour. In FIG. 3c we show  $\xi_p^a/\xi_p$  as a function of  $Pe$  for a range of bare bending stiffnesses. For low values of  $Pe$ ,  $\xi_p^a/\xi_p$  remains close to 1, indicating that the filament stiffness is not affected by activity. However, as the activity increases, one observes a rapid decrease of the persistence length. This activity-driven reduction of  $\xi_p^a$  is accompanied by a drop in the radius of gyration (FIG. 3c, inset), indicating that the system transitions into a coiled state.

In order to characterise the spiralling state, we computed the average angular velocity of filaments around their centres of mass. The instantaneous angular velocity of filament  $j$  was calculated as  $\boldsymbol{\omega}_j(t) = 1/N \sum_{i=1}^N (\mathbf{r}_i(t) - \mathbf{r}_{j,cm}(t)) \times (\mathbf{v}_i(t) - \mathbf{v}_{j,cm}(t)) / |\mathbf{r}_i(t) - \mathbf{r}_{j,cm}(t)|^2$ , where  $\mathbf{r}_i(t)$  and  $\mathbf{v}_i(t)$  are, respectively, the position and velocity of the bead  $i$  at time  $t$ . Similarly,  $\mathbf{r}_{j,cm}(t)$  and  $\mathbf{v}_{j,cm}(t)$  are the instantaneous position and velocity of the centre of mass of filament  $j$ , respectively. The average magnitude of the angular velocity per filament was computed as  $\omega = 1/M \sum_{j=1}^M |1/\tau_m \sum_t \boldsymbol{\omega}_j(t)|$ , where  $\tau_m$  is the measurement time. We note that the order in which averages are taken is important to properly capture rotations of individual filaments, and also that  $\omega$  retains a small but finite plateau at low  $Pe$ . In FIG. 3d we show that  $\omega$  increases sharply from its plateau value as a function of



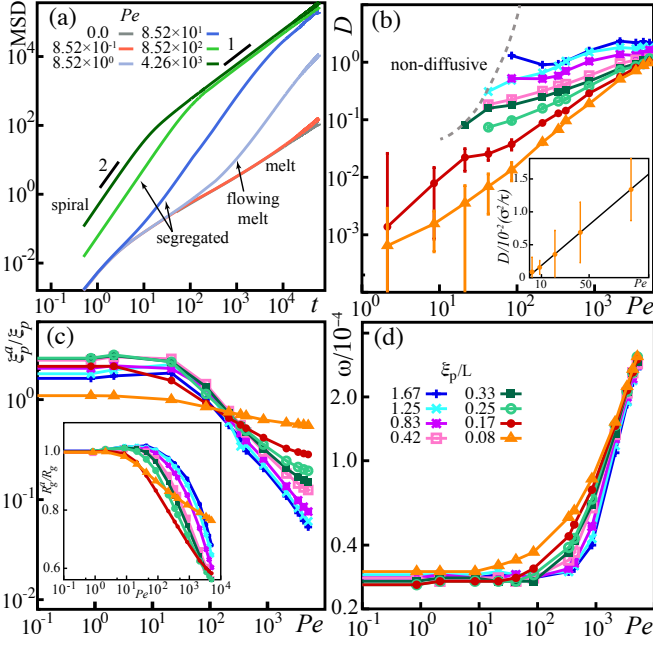


FIG. 3. (Colour online) (a) Mean-squared displacement (MSD) as a function of time for  $\xi_p/L \approx 0.83$  for four values of  $Pe$ . (b) Log-log plot of the diffusion coefficient as a function of  $Pe$  in the regime where the system is diffusive. *Inset*: Linear plot at low activity for a soft ( $\xi_p/L = 0.08$ ) filament. (c) Ratio of active ( $\xi_p^a$ ) to passive ( $\xi_p = 2\kappa b/k_B T$ ) persistence length for a range of values of bare bending stiffnesses. Note that due to steric repulsions for low activity the measured persistence length is always larger than  $\xi_p$ . *Inset*: Ratio of active,  $R_g^a$ , to passive,  $R_g$ , radius of gyration as a function of  $Pe$ . (d) Average angular velocity of rotation around centres of mass of filaments as a function of  $Pe$ . Legend in (d) also applies to panels (b) and (c).  $N = 25$  in all plots.

Péclet number as the buckling threshold is crossed, confirming that individual spirals rotate. The rate of the increase of  $\omega$  with  $Pe$  grows with filaments stiffness, which is not surprising as softer filaments are easier to bend.

Finally, we explore how orientational order of semi-flexible filaments emerges from self-propulsion. Steric repulsion leads to local alignment which does not depend on the filament direction and, therefore, has nematic symmetry. On the other hand, self-propulsion introduces directionality, i.e., filament polarity. Therefore, we compute both polar and nematic local order parameter of the filament bond vectors connecting consecutive beads. The order parameter is  $S_m = \langle \cos(m\theta) \rangle$ , with  $\theta$  being the angle between a pair of bond vectors sharing a bead, and  $m = 1$  for polar,  $m = 2$  for nematic. The average  $\langle \cdot \rangle$  is over all the pairs within a cut-off distance,  $5\sigma$ .

In FIG. 4a we show the local polar order parameter  $S_1$  as a function of  $Pe$ . For low  $Pe$ , the effects of activity are very weak and there is essentially no polar ordering. As the activity is increased, filaments align their propulsion directions and start to flow as a bundle, leading to

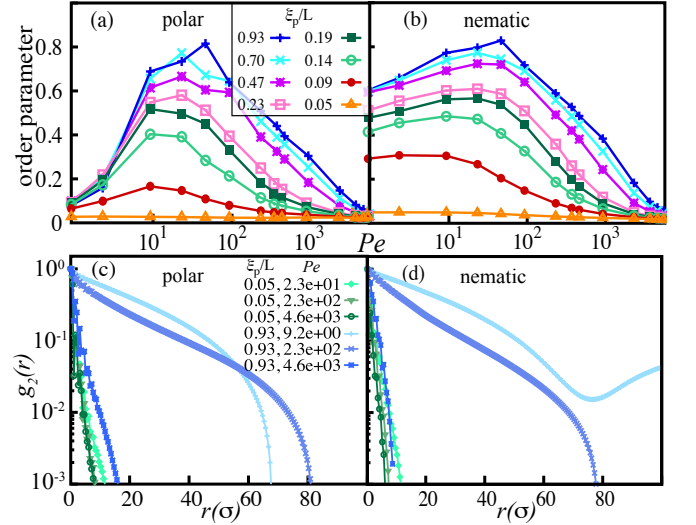


FIG. 4. (Colour online) Local polar (a) and nematic (b) order parameter as a function of activity for a range of bare filament stiffnesses for  $N = 25$ . Spatial correlation function  $g_{m,2}(r)$  for the polar (c) and nematic (d) order parameter. The upturn in (d) is an artefact of averaging for large  $r$ .

a boost in  $S_1$  for the intermediate values of  $Pe$ . At large activities, the system collapses into the spiralling phase, and the order disappears. We observe similar behaviour for the local nematic order  $S_2$  (FIG. 4b). The main difference is that at low activity the system exhibits substantial local nematic order, consistent with the passive polymer melt [18].

In order to probe the extent of the local order in FIG. 4c&d we show the spatial pair-correlations of both polar and nematic order parameters. These correlation functions are defined as  $g_{m,2}(r) = \langle \sum_{i,j}^{i>j} \delta(r - |r_i - r_j|) \cos(m\theta_{ij}) \rangle / \langle \sum_{i,j}^{i>j} \delta(r - |r_i - r_j|) \rangle$ . In all regimes, we observed an exponential decay of  $g_{m,2}$ . There is, however, a clear difference between flexible and stiff filaments in terms of the extent of spatial correlations. For flexible filaments the order is indeed local and  $g_{m,2}$  rapidly drops to zero at distances  $\sim 10\sigma$ . However, for stiff filaments, both polar and nematic order persist over much longer distances, reaching 1/5-th of the system size. In the high activity regime, coiling into spirals, however, completely destroys the order even for the stiffest filaments.

In summary, we used Langevin dynamics simulations to map a detailed non-equilibrium phase diagram of a two-dimensional melt of self-propelled semi-flexible filaments. We found that the activity has profound effects on the collective behaviour of dense suspensions of filaments leading to a number of interesting phenomena, including the onset of a weakly interacting spiralling state at high activity, which has no analogue in systems of structureless active agents. It would be interesting to fully characterise the nature of the flowing melt phase, where one observes spontaneous formation of half-integer topologi-

cal defects. Specifically, it would be intriguing to explore if the topological defect develop orientational order akin to that seen in the experiments on active microtubules [5]. In our simulations we were unable to observe any evidence of such ordering. We speculate that this is due to the time scales accessible to our simulations, with far longer runs required to properly characterise this regime of very slow dynamics.

*Acknowledgements.* We acknowledge financial support from EPSRC (EP/M009599/1) and BBSRC (BB/N009789/1 and BB/N009150/1). We thank A. Das for comments on the manuscript. KRP would like to thank A. Maitra and S. Saha for many useful discussions.

---

\* r.sknepek@dundee.ac.uk

- [1] M. Marchetti, *et al.*, Rev. Mod. Phys. **85**, 1143 (2013).
- [2] S. Ramaswamy, Annu. Rev. Condens. Matter Phys. **1**, 323 (2010).
- [3] T. Sanchez, *et al.*, Nature **491**, 431 (2012).
- [4] F. C. Keber, *et al.*, Science **345**, 1135 (2014).
- [5] S. J. DeCamp, *et al.*, Nat. Mater. **14**, 1110 (2015).
- [6] L. Giomi, M. J. Bowick, X. Ma, and M. C. Marchetti, Phys. Rev. Lett. **110**, 228101 (2013).
- [7] S. P. Thampi, R. Golestanian, and J. M. Yeomans, Phys.

- Rev. Lett. **111**, 118101 (2013).
- [8] G. Jayaraman, *et al.*, Phys. Rev. Lett. **109**, 158302 (2012).
- [9] H. Jiang and Z. Hou, Soft Matter **10**, 1012 (2014).
- [10] R. E. Isele-Holder, J. Elgeti, and G. Gompper, Soft Matter **11**, 7181 (2015).
- [11] A. Baskaran and M. C. Marchetti, Phys. Rev. Lett. **101**, 268101 (2008).
- [12] A. Peshkov, *et al.*, Phys. Rev. Lett. **109**, 268701 (2012).
- [13] K. Sekimoto, N. Mori, K. Tawada, and Y. Y. Toyoshima, Phys. Rev. Lett. **75**, 172 (1995).
- [14] L. Bourdieu, *et al.*, Phys. Rev. Lett. **75**, 176 (1995).
- [15] R. Chelakkot, A. Gopinath, L. Mahadevan, and M. F. Hagan, J. R. Soc. Interface **11**, 20130884 (2013).
- [16] T. B. Liverpool, Phys. Rev. E **67**, 031909 (2003).
- [17] A. Ghosh and N. S. Gov, Biophys. J **107**, 1065 (2014).
- [18] M. Doi and S. F. Edwards, *The theory of polymer dynamics*, (Oxford university press, 1988).
- [19] M. E. Cates and J. Tailleur, Ann. Rev. Cond. Matt. Phys. **6**, 219 (2015).
- [20] G. S. Redner, M. F. Hagan, and A. Baskaran, Phys. Rev. Lett. **110**, 055701 (2013).
- [21] K. Kremer and G. S. Grest, J. Chem. Phys. **92**, 5057 (1990).
- [22] J. D. Weeks, D. Chandler, and H. C. Andersen, J. Chem. Phys. **54**, 5237 (1971).
- [23] S. Plimpton, J. Chem. Phys. **117**, 1 (1995).
- [24] Supplemental material available at: [URL will be inserted by publisher].

## Supplemental Materials: Dynamically Generated Patterns in Dense Suspensions of Active Filaments

### A - NORMAL MODE ANALYSIS OF AN ACTIVE ROUSE CHAIN

Here we use a standard normal mode analysis of the Rouse model [S1] to analyse the effects of the active force applied along the contour of the filament. Normal mode analysis of the dynamics of a semi-flexible filament involves solving a fourth order equation for the normal modes [S2] and is not entirely straightforward. Extending it to take into account effects of the activity leads to a number of technical complications. Gosh and Gov [S3] recently performed normal mode analysis of an active semi-flexible filament with the activity introduced as time correlated noise. Unfortunately, a similar analysis performed on the activity modelled in this paper leads to analytically intractable equations for normal mode frequencies and is not overly insightful.

Instead, here we study the simpler problem of the Rouse model dynamics of an active flexible polymer. We focus on the weak activity ( $Pe \lesssim 1$ ), weak rigidity limit ( $\xi_P/L \lesssim 10^{-1}$ ), i.e., in the lower left corner on the phase diagram in FIG. 1 in the main text, where the assumption of a fully flexible chain is justifiable. The model is easily analytically tractable and leads to some insightful observations. We note that for sufficiently short polymers over sufficiently low time scales, the Rouse model accurately captures chain dynamics in the melt state [S4].

#### Rouse chain with active force along its contour

In the Rouse model [S1] a filament is represented as a chain of  $N$  beads connected via harmonic springs of stiffness  $k$ . The chain is fully flexible and excluded volume and hydrodynamic interactions are neglected. The Langevin equation for bead  $n$  is

$$\gamma \frac{d\mathbf{r}_n}{dt} = -k(2\mathbf{r}_n - \mathbf{r}_{n+1} - \mathbf{r}_{n-1}) + \mathbf{R}_n, \quad (\text{S1})$$

for  $n = 2, \dots, N - 1$  and

$$\gamma \frac{d\mathbf{r}_1}{dt} = -k(\mathbf{r}_1 - \mathbf{r}_2) + \mathbf{R}_1 \quad (\text{S2})$$

$$\gamma \frac{d\mathbf{r}_N}{dt} = -k(\mathbf{r}_N - \mathbf{r}_{N-1}) + \mathbf{R}_N, \quad (\text{S3})$$

where  $\gamma$  is the friction coefficient and  $\mathbf{R}_n$  is a random force with zero mean and variance, i.e.,

$$\begin{aligned} \langle \mathbf{R}_n(t) \rangle &= 0, \\ \langle R_{n,\alpha}(t) R_{m,\beta}(t') \rangle &= 2k_B T \gamma \delta_{nm} \delta_{\alpha\beta} \delta(t - t'), \end{aligned} \quad (\text{S4})$$

where  $\alpha, \beta \in \{x, y\}$  for a two-dimensional system. It is convenient to treat bead index  $n$  as a continuous variable and write Eqs. (S1)-(S3) as a partial differential equation [S1],

$$\gamma \frac{\partial \mathbf{r}(n, t)}{\partial t} = k \frac{\partial^2 \mathbf{r}(n, t)}{\partial n^2} + \mathbf{R}(n, t), \quad (\text{S5})$$

with boundary conditions

$$\left. \frac{\partial \mathbf{r}}{\partial n} \right|_{n=0} = \left. \frac{\partial \mathbf{r}}{\partial n} \right|_{n=N} = 0. \quad (\text{S6})$$

In our model the active force acts along the contour of the filament and can be written as

$$\mathbf{F}_a(n) = f_p \mathbf{t}(n), \quad (\text{S7})$$

where

$$\mathbf{t}(n) = \frac{\partial \mathbf{r}}{\partial n}$$

is the tangent vector. The equation of motion for the filament can be obtained by adding the term in Eq. (S7) to Eq. (S5)

$$\gamma \frac{\partial \mathbf{r}(n, t)}{\partial t} = f_p \frac{\partial \mathbf{r}(n, t)}{\partial n} + k \frac{\partial^2 \mathbf{r}(n, t)}{\partial n^2} + \mathbf{R}(n, t). \quad (\text{S8})$$

We assume that the filament ends are free leading to the boundary conditions in Eq. (S6). We seek for solutions of Eq. (S8) in the form

$$\mathbf{X}_p(t) = \int_0^N dn \phi_p(n) \mathbf{r}(n, t), \quad (\text{S9})$$

where  $\mathbf{X}_p(t)$  satisfies equation

$$\gamma_p \frac{d\mathbf{X}_p}{dt} = -k_p \mathbf{X}_p + \mathbf{R}_p(t), \quad (\text{S10})$$

with coefficients  $\gamma_p$  and  $k_p$  that will have to be related to  $\gamma$  and  $k$  in Eq. (S5). The effective noise on mode  $p$  is formally given as

$$\mathbf{R}_p(t) = \frac{\gamma_p}{\gamma} \int_0^N dn \phi_p(n) \mathbf{R}(n, t). \quad (\text{S11})$$

Inserting Eq. (S9) into Eq. (S10) leads to equations for the modes  $\phi_p(n)$ ,

$$k \frac{d^2 \phi_p(n)}{dn^2} - f_p \frac{d\phi_p(n)}{dn} = -\frac{k_p \gamma}{\gamma_p} \phi_p(n), \quad (\text{S12})$$

with the boundary conditions

$$\left[ f_p \phi_p(n) - k \frac{d\phi_p(n)}{dn} \right]_{n=0} = \left[ f_p \phi_p(n) - k \frac{d\phi_p(n)}{dn} \right]_{n=N} = 0. \quad (\text{S13})$$

Solutions of Eq. (S12) are of the form

$$\phi_p(n) = Ae^{i\omega n}, \quad (\text{S14})$$

which when inserted into Eq. (S12) leads to

$$\left(-k\omega^2 - f_p i\omega + \frac{k_p \gamma}{\gamma_p}\right) Ae^{i\omega n} = 0. \quad (\text{S15})$$

This equation has a non-trivial solution if

$$k\omega^2 + f_p i\omega - \frac{k_p \gamma}{\gamma_p} = 0. \quad (\text{S16})$$

We solve Eq. (S16) to find

$$\omega_1 = -i\frac{f_p}{2k} + \omega_p \quad (\text{S17})$$

$$\omega_2 = -i\frac{f_p}{2k} - \omega_p, \quad (\text{S18})$$

where

$$\omega_p = \sqrt{\frac{k_p \gamma}{k \gamma_p}} \left(1 - \frac{f_p^2 \gamma_p}{4k k_p \gamma}\right)^{1/2}. \quad (\text{S19})$$

Therefore, the most general solution of Eq. (S12) is

$$\phi_p(n) = e^{\frac{f_p}{2k}n} (Ae^{i\omega_p n} + Be^{-i\omega_p n}), \quad (\text{S20})$$

where  $A$  and  $B$  are yet to be determined constants.

### Limit of weak activity

We will assume that the activity is weak, i.e. that  $\frac{f_p N}{k} \ll 1$ . We can take the formal derivative of Eq. (S20) to obtain

$$\frac{d\phi_p(n)}{dn} = \frac{f_p}{2k} e^{\frac{f_p}{2k}n} (Ae^{i\omega_p n} + Be^{-i\omega_p n}) + e^{\frac{f_p}{2k}n} i\omega_p (Ae^{i\omega_p n} - Be^{-i\omega_p n}). \quad (\text{S21})$$

Substituting Eq. (S21) into the equation (Eq. (S13)) for boundary conditions leads to

$$\begin{aligned} \left(\frac{f_p}{2} - ik\omega_p\right) A + \left(\frac{f_p}{2} + ik\omega_p\right) B &= 0 \\ \left(\frac{f_p}{2} - ik\omega_p\right) e^{i\omega_p N} A + \left(\frac{f_p}{2} + ik\omega_p\right) e^{-i\omega_p N} B &= 0. \end{aligned} \quad (\text{S22})$$

In order for this system of equations to have a non-trivial solutions, its determinant has to be zero and the following condition has to be satisfied,

$$-2i \left( \left( \frac{f_p}{2} \right)^2 + k^2 \omega_p^2 \right) \sin \omega_p N = 0.$$

Since  $\omega_p$  is real, the only solution of this equation is

$$\omega_p = \frac{\pi p}{N}, \quad (\text{S23})$$

for  $p = 0, 1, 2, \dots$ . This expression together with Eq. (S19) leads to the equation for the mode stiffness

$$k_p = \frac{k \gamma_p}{\gamma} \left( \frac{\pi p}{N} \right)^2 \left( 1 + \left( \frac{f_p N}{2k \pi p} \right)^2 \right). \quad (\text{S24})$$

This is an interesting result as it shows that the modes become stiffer with activity. We recall that this calculation is for a fully flexible model and this mode stiffening should not be confused with the reduction of the persistence length discussed in the main text which is an effect related to the bending stiffness of the chain, which is ignored here.

From the first line in Eq. (S22) we readily see that

$$B = -\frac{(f_p - 2ik\omega_p)}{(f_p + 2ik\omega_p)}A. \quad (\text{S25})$$

If we take the limit  $f_p \rightarrow 0$  in the last expression we recover a familiar result of the Rouse theory [S1],  $B = A$ . However, for finite  $f_p$  the  $p = 0$  mode requires  $B = -A$ , indicating a sine-like solution, i.e.,  $\phi_p(n) = Ae^{\frac{f_p}{2k}n} \sin \omega_p n$ , which is identically equal to zero for  $p = 0$ . This already suggests that the  $p = 0$  mode is special, which is not surprising as the activity adds a persistence to otherwise diffusive motion. The  $p = 0$  mode is, however, important for calculating the diffusion coefficient of the centre of mass, which is what we set out to do. For the purpose of this demonstration, we will therefore continue our argument by making a set of rather strong assumptions that would require a proper justification in a full calculation.

It is straightforward to show that the solution of Eq. (S12) can be written as

$$\phi_p(n) = 2A \left(1 + \frac{f_p}{2k}n\right) \cos \omega_p n + Ai \frac{f_p}{k} \frac{1}{\omega_p} e^{-i\omega_p n}, \quad (\text{S26})$$

valid for all  $p > 0$ . It is immediately evident that the last term in Eq. (S26) diverges for  $p = 0$ . For the sake of the argument we, however, assume that activity acts as a weak perturbation to the diffusive motion (an assumption consistent with the empirical observations in our simulations) and write the approximate solution as

$$\phi_p(n) \approx 2A \left(1 + \frac{f_p}{2k}n\right) \cos \omega_p n, \quad (\text{S27})$$

assuming it to be valid for all  $p \geq 0$ . In the limit  $f_p \rightarrow 0$  we obtain

$$\phi_p(s) = 2A \cos \omega_p n,$$

thus suggesting that we can choose

$$A = \frac{1}{2N}.$$

Therefore,

$$\mathbf{X}_p(t) \approx \frac{1}{N} \int_0^N dn \left(1 + \frac{f_p}{2k}n\right) \cos(\omega_p n) \mathbf{r}(n, t). \quad (\text{S28})$$

### Noise correlation function

We proceed to compute variance of the random force  $\langle \mathbf{R}_p(t) \cdot \mathbf{R}_q(t') \rangle$ . Using Eq. (S11),

$$\langle R_{p,\alpha}(t) R_{q,\beta}(t') \rangle = 2k_B T \frac{\gamma_p \gamma_q}{\gamma} \delta_{\alpha\beta} \delta(t - t') \int_0^N dn \phi_p(n) \phi_q(n), \quad (\text{S29})$$

where  $\alpha, \beta \in \{x, y\}$ . Here we have assumed that the fluctuation-dissipation theorem is still valid, as long as the perturbations introduced by the active forces are small compared to the thermal fluctuations. We can compute the integral using Eq. (S27) which gives,

$$\int_0^N dn \phi_p(n) \phi_q(n) = \frac{N^2}{\pi^2} \frac{(p^2 + q^2)}{(p^2 - q^2)^2} \begin{cases} 0 & \text{if } p + q \text{ even} \\ -2 & \text{if } p + q \text{ odd} \end{cases}, \quad (\text{S30})$$

which is valid for  $p \neq q$ . For  $p = q$  we have

$$I = \int_0^N dn n \cos^2\left(\frac{p\pi}{L}n\right) = \frac{1 + \delta_{p,0}}{4} N^2. \quad (\text{S31})$$



For  $p = q$  we have

$$\langle R_{p,\alpha}(t) R_{p,\beta}(t') \rangle = k_B T \frac{\gamma_p^2}{\gamma} \delta_{\alpha\beta} \delta(t-t') \frac{1 + \delta_{p,0}}{N} \left[ 1 + \frac{f_p N}{2k} \right].$$

If we now request

$$\langle R_{p,\alpha}(t) R_{p,\beta}(t') \rangle = 2k_B T \gamma_p \delta_{\alpha\beta} \delta(t-t'),$$

we can read off

$$\gamma_p = \frac{2\gamma N}{1 + \delta_{p,0}} \frac{1}{1 + \frac{f_p N}{2k}} \approx \frac{2\gamma N}{1 + \delta_{p,0}} \left( 1 - \frac{f_p N}{2k} \right). \quad (\text{S32})$$

Indicating that activity reduces the noise. Finally,

$$\langle R_{p,\alpha}(t) R_{p,\beta}(t') \rangle = 2k_B T \frac{2\gamma N}{1 + \delta_{p,0}} \left( 1 - \frac{f_p N}{2k} \right) \delta_{\alpha\beta} \delta(t-t'), \quad (\text{S33})$$

For  $p \neq q$  we have

$$\langle R_{p,\alpha}(t) R_{q,\beta}(t') \rangle = -4k_B T \frac{\gamma_p \gamma_q}{\gamma} \frac{f_p}{k\pi^2} \frac{(p^2 + q^2)}{(p^2 - q^2)^2} G(p+q) \delta_{\alpha\beta} \delta(t-t'),$$

where

$$G(p+q) = \begin{cases} 0 & \text{if } p+q \text{ even} \\ 1 & \text{if } p+q \text{ odd} \end{cases}.$$

If we now use Eq. (S32) we obtain

$$\frac{\gamma_p \gamma_q}{\gamma} \approx \frac{4\gamma N^2}{(1 + \delta_{p,0})(1 + \delta_{q,0})} \left( 1 - \frac{f_p N}{k} \right),$$

which leads to (for  $p \neq q$ ),

$$\langle R_{p,\alpha}(t) R_{q,\beta}(t') \rangle \approx -\frac{16N}{\pi^2} k_B T \gamma \frac{f_p N}{k} \frac{(p^2 + q^2)}{(p^2 - q^2)^2} G(p+q) \delta_{\alpha\beta} \delta(t-t'). \quad (\text{S34})$$

This equation shows that noise modes are not independent of each other indicating that activity causes interesting correlation effects in the noise term essentially invalidating the fluctuation-dissipation theorem.

### Centre of mass diffusion

In order to compute the centre of mass diffusion coefficient, we need to compute the mean squared displacement (MSD). This is achieved by noting that we can write

$$\mathbf{r}(n, t) \approx \mathbf{X}_0(t) \left( 1 - \frac{f_p}{2k} n \right) + 2 \sum_{q=1}^{\infty} \left( 1 - \frac{f_p}{2k} n \right) \cos(\omega_q n) \mathbf{X}_q(t). \quad (\text{S35})$$

$\mathbf{X}_q(t)$  can be directly evaluated [S1] to give

$$\mathbf{X}_q(t) = \frac{e^{-\frac{k_p}{\gamma_p} t}}{\gamma_p} \int_0^t dt' e^{\frac{k_p}{\gamma_p} t'} \mathbf{R}_p(t'). \quad (\text{S36})$$

For the MSD we only need to know the time dependence of the lowest,  $p = 0$  mode. It is easy to show that to the leading order in  $f_p N/k$  this mode is

$$\mathbf{X}_0(t) \approx \frac{1}{\gamma N} \left( 1 + \frac{f_p N}{2k} \right) \int_0^t dt' \mathbf{R}_0(t').$$

This directly leads to

$$\left\langle \left( \vec{X}_0(t) \right)^2 \right\rangle \approx \frac{4k_B T}{\gamma N} \left( 1 + \frac{f_p N}{2k} \right) t, \quad (\text{S37})$$

which allows us to define the activity dependent diffusion coefficient

$$D_t(f_p) = \frac{k_B T}{\gamma N} \left( 1 + \frac{f_p N}{2k} \right), \quad (\text{S38})$$

indicating that, to the leading order in activity, the diffusion coefficient for the centre of mass increases linearly with activity.

We note that this theory should only be considered as a qualitative demonstration of the effects of activity on a filament. The calculation is quite crude and involves many approximations, most notably the assumption that in the  $p = 0$  mode we can assume activity to simply acts as a weak perturbation of the diffusive motion.

An alternative approach would be to treat the  $p = 0$  mode separately from the outset, by deriving equation for the centre of mass motion. We define

$$\mathbf{X}_0(t) = \frac{1}{N} \int_0^N dn \mathbf{r}(n, t).$$

We can derive the separate equation

$$\frac{\gamma}{N} \int_0^N dn \frac{\partial \mathbf{r}(n, t)}{\partial t} = \frac{f_p}{N} \int_0^N dn \frac{\partial \mathbf{r}(n, t)}{\partial n} + \frac{k}{n} \int_0^N dn \frac{\partial^2 \mathbf{r}(n, t)}{\partial n^2} + \frac{1}{N} \int_0^N dn \mathbf{R}(n, t). \quad (\text{S39})$$

The left hand side is simply  $\frac{\partial \mathbf{X}_0(t)}{\partial t}$ . On the right hand side, the second term disappears because of the boundary conditions Eq. (S6). The noise term can be computed in a straightforward manner. If we define  $\mathbf{R}_0(t) = \frac{1}{N} \int_0^N dn f(n, t)$ , we have

$$\langle \mathbf{R}_0(t) \cdot \mathbf{R}_0(t') \rangle = 4k_b T \frac{\gamma}{N} \delta(t - t'). \quad (\text{S40})$$

The first term on the right hand side can be formally written as an effective active force

$$\mathbf{F}_0 = \frac{f_p}{N} (\mathbf{r}(N, t) - \mathbf{r}(0, t)). \quad (\text{S41})$$

Then the equation for the centre of mass can be written as

$$\gamma \frac{\partial \mathbf{X}_0(t)}{\partial t} = \mathbf{F}_0(t) + \mathbf{R}_0(t). \quad (\text{S42})$$

Since we have subtracted the persistent part of the motion, the Rouse calculation applies now to  $\mathbf{F}_0$ . By using Eq. (S10) for the equation of motion, Eq. (S24) for the stiffness, Eq. (S32) for the friction coefficient and Eq. (S33) for the noise we obtain

$$\gamma_p \frac{\partial \mathbf{F}_0}{\partial t} = f_p \mathbf{R}_0,$$

with  $\gamma_p = \gamma N$  and  $\mathbf{R}_p = \sqrt{N} \mathbf{R}$ . Finally, we end with a very simple diffusive process for this term,

$$\frac{\partial \mathbf{F}_0}{\partial t} = \frac{f_p}{\gamma} \mathbf{R}(t). \quad (\text{S43})$$

This means that the effective active force term for the centre of mass is akin to the active self-propulsion term  $v_0 \hat{\mathbf{n}}$  in a common model of self-propelled disks [S5]. The dynamics of  $\mathbf{F}_0$  itself is diffusive, with a diffusion constant  $\nu_F = 2k_b T \gamma$ . Note that this is a wholly distinct quantity from the rotational diffusion of a thermal polymer. This is very interesting because Eq. (S42) is now an equation for a persistent random walk, with an additional thermal component.

We can solve this equation and obtain the following mean-squared displacement [S5]

$$\langle (\mathbf{X}_0(t) - \mathbf{X}_0(0))^2 \rangle = 4 \frac{f_p^2}{2\nu_F} \left( t + \frac{1}{\nu_F} (e^{-\nu_F t} - 1) \right) + 4k_b T / \gamma N. \quad (\text{S44})$$

In the long-time limit, this means the centre-of-mass diffuses with diffusion coefficient

$$D_{f_p} = 4k_bT/\gamma N + \frac{f_p^2}{k_bT\gamma}. \quad (\text{S45})$$

When comparing to Eq. (S38), we see that we have acquired an additional term  $\frac{f_p^2}{k_bT\gamma}$  that is quadratic in  $f_p$  and stems from the persistent part of the active motion. This term is very similar to the additional diffusion term  $D_{\text{act}} = \frac{v_0^2}{2\nu_r}$  (where  $v_0$  is the self-propulsion speed and  $\nu_r$  is the rotational friction coefficient) that can be derived for system of self-propelled particles without internal degrees of freedom.

This suggests that the diffusion coefficient scales as a square of the activity, which is, unfortunately, not consistent with the simulations.

Both calculations show that the effects of activity on filament dynamics are not trivial and require a much more careful calculation to fully understand.

## B - SPATIAL CORRELATION FUNCTION OF THE CHAIN HEADS

We observe that during “flocking”, heads of individual chains aggregate together and move forward. Therefore, measuring the pair correlation function of the head-beads of each filament is relevant to understanding the clustering. In Fig. S1a we show the head-head pair correlation. Oscillations in  $g(r)$ , prior to approaching the asymptotic value 1, show a phase co-existence. In the “rotating spirals” regime the first small “kink” corresponds to  $R_g$  of the filament, where the centre of mass of the filament is approximately equal to the position of the head of the chain. In this phase, high  $\kappa$  values shows oscillations around 1, suggesting that clustering is negligible.  $g(r)$  in the “swirling” phase does not show any peculiar behaviour as it is a mixed phase of extended and coiled polymers.

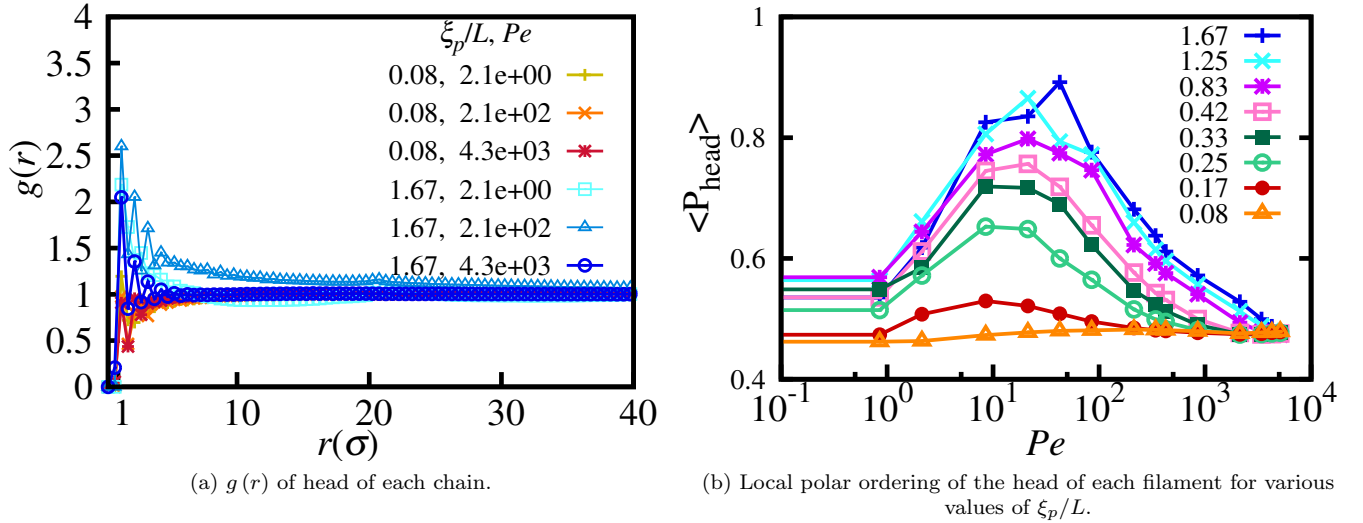
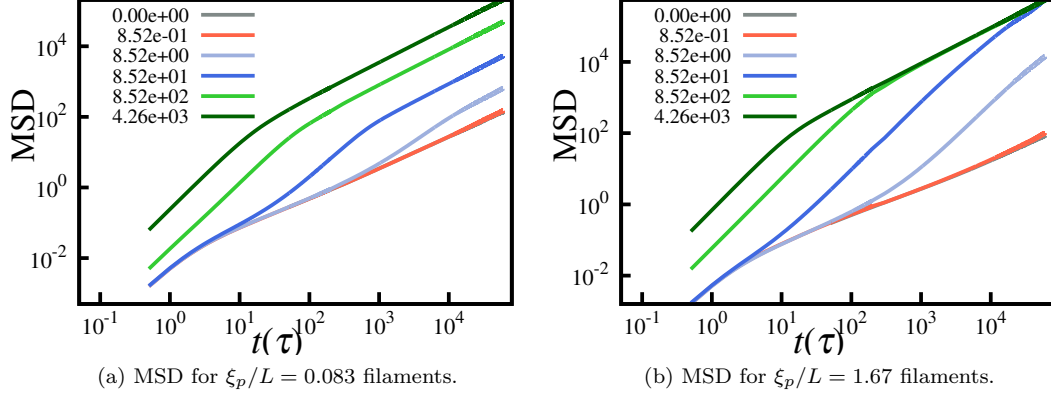
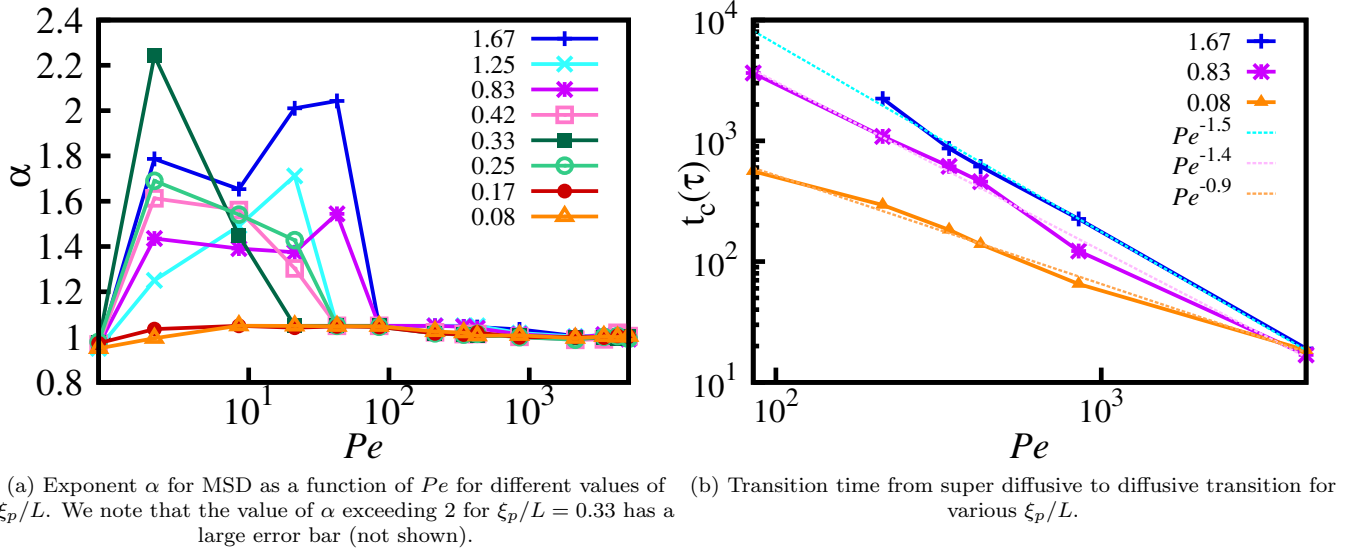


FIG. S1. Spatial correlation and polar ordering of heads of filaments.

## C - POLAR ORDERING OF FILAMENT HEADS

We clearly observe ordering of heads in the flocking phase. We quantify this by measuring the local ordering of heads in the filament. Fig. S1b shows polar ordering of polymer heads, suggesting that filaments move in same direction in a given cluster.

FIG. S2. Mean squared displacement curves for different values of  $Pe$  (legends).FIG. S3. MSD exponent  $\alpha$  and crossover time  $t_c$ .

#### D - MEAN SQUARED DISPLACEMENT

We measure the mean squared displacement (MSD) of the centre of mass of the filament  $i$ . For long times, the MSD grows with time as a power law,

$$\langle (X_i(t) - X_i(0))^2 \rangle \propto t^\alpha. \quad (\text{S46})$$

The value of the exponent  $\alpha$  determines the nature of the dynamics, with  $\alpha = 2$  being persistent (ballistic),  $1 < \alpha < 2$  superdiffusive,  $\alpha = 1$  diffusive, and  $\alpha < 1$  sub-diffusive. In Fig. S2 we show the MSD plot for two different  $\xi_p/L$  values. Fig S3a shows the value of  $\alpha$  for various values of  $\xi_p/L$  and  $Pe$ .

Fig. S3a shows that value of this exponent for various  $\xi_p/L$  and  $Pe$  values.

It is immediately clear that there is a cross over from ballistic to diffusive behaviour for  $Pe \gtrsim 10^2$ . We measured this cross over time  $t_c$  for different cases. This shows a power law behaviour ( $Pe^{-\zeta}$ ), with exponent  $\zeta$  varying between 0.9 and 1.5. Figure S3b shows cross over time for different  $\xi_p/L$  values.

#### E - MOVIES

In all movies, filaments are color-coded by their indices.

### Movies describing various phases

**movie1.mp4:** Langevin dynamics simulation of **melt phase** with  $\xi_p/L = 1.67$  with  $N = 25$  and  $Pe = 2.1$ .

**movie2.mp4:** Langevin dynamics simulation of **co-existence phase** with  $\xi_p/L = 1.67$  with  $N = 25$  and  $Pe = 85.20$ .

**movie3.mp4:** Langevin dynamics simulation of **flowing melt** with  $\xi_p/L = 0.33$  with  $N = 25$  and  $Pe = 8.520$ . Note that the movie was considerably sped up for the flow to be clearly visible.

**movie4.mp4:** Langevin dynamics simulation of **swirls** with  $\xi_p/L = 0.17$  with  $N = 25$  and  $Pe = 85.20$ .

**movie5.mp4:** Langevin dynamics simulation of the **rotating spiral** phase with  $\xi_p/L = 0.04$  with  $N = 50$  and  $Pe = 17757.8$ . Red bead is head of each filament.

**movie6.mp4:** Langevin dynamics simulation, showing that there is no spiral formation in short filament case  $N = 5$   $\xi_p/L = 0.5$  with  $Pe = 118.34$ .

### Low density movies

In addition, in order to further explore the collective behaviour in the system, we performed several low density ( $\phi = 0.064$  and  $0.16$ ) simulations.

**movie7.mp4:** Langevin dynamics simulation showing cluster formation and breaking in the segregated phase at  $\phi = 0.16$ ,  $\xi_p/L = 1.67$  with  $N = 25$  and  $Pe = 85.20$ .

**movie8.mp4:** Langevin dynamics simulation depicting cluster formation from a random filament configuration  $\phi = 0.064$ ,  $\xi_p/L = 4.081$  with  $N = 50$  and  $Pe = 1775.78$ .

**movie9.mp4:** Spiral formation in the low density regime  $\phi = 0.064$ ,  $\xi_p/L = 0.0041$  with  $N = 50$  and  $Pe = 17757.8$ .

### Without Self-avoidance

We performed several simulations to understand the effect of self-avoidance. We see that clustering as well as spiralling is absent when self-avoidance is absent.

**movie10.mp4:** No spiral formation  $\phi = 0.064$ ,  $\xi_p/L = 0.0041$  with  $N = 50$  and  $Pe = 17757.8$ .

---

\* r.sknepnek@dundee.ac.uk

- [S1] Doi, M. and Edwards, S. F., *The theory of polymer dynamics*, Oxford University Press (1988)
- [S2] Aragon, S.R and Pecora, R., *Macromolecules* **18**, 1868 (1985).
- [S3] Gosh, A. and Gov N. S., *Biophysical Journal* **107**, 1065 (2014).
- [S4] Chatterjee, A. P. and Loring R. F., *Journal of Chemical Physics* **101**, 1595 (1994).
- [S5] Fily, Y., Henkes, S. and M. Cristina Marchetti, *Soft Matter* **10**, 2132 (2014).